# Raman and mid-infrared spectroscopic study of geometrically frustrated hydroxyl cobalt halides at room temperature*

Liu Xiao-Dong(刘晓东)[a)†], Meng Dong-Dong(孟冬冬)[a)], Hagihala Masato(萩原雅人)[a)], Zheng Xu-Guang(郑旭光)[a)b)], and Guo Qi-Xin(郭其新)[c)]

[a)] *Department of Physics, Graduate School of Science and Engineering, Saga University, Saga* 840-8502, *Japan*

[b)] *Department of Physics, Faculty of Science and Engineering, Saga University, Saga* 840-8502, *Japan*

[c)] *Synchrotron Light Application Center & Department of Electrical and Electronic Engineering, Saga University, Saga* 840-8502, *Japan*

(Received 25 November 2010; revised manuscript received 16 March 2011)

Mid-infrared absorption and Raman spectra of the geometrically frustrated material series, hydroxyl cobalt halides β-$Co_2(OH)_3Cl$ and β-$Co_2(OH)_3Br$, are first, to the best of our knowledge, measured at room temperature, to study the corresponding relationship between their vibrational spectral properties and crystal microstructures. Through the comparative analysis of the four spectra we have categorically assigned the OH-related vibration modes of hydroxyl groups in the trimeric hydrogen bond environment ($Co_3 \equiv OH)_3 \cdots Cl/Br$, and tentatively suggested vibration modes of O–Co–O, Co–O and Cl/Br–Co–Cl/Br units. These results can also become the basis for analysing their low-temperature spectral properties, which can help to understand the underlying physics of their exotic geometric frustration phenomena around phase transition temperatures.

**Keywords:** geometrical frustration, hydroxyl cobalt chloride, hydroxyl cobalt bromide, trimeric hydrogen bond

**PACS:** 78.30.–j, 33.20.Ea, 61.66.Fn **DOI:** 10.1088/1674-1056/20/7/077801

## 1. Introduction

After our group first (to the best of our knowledge) pointed out that three isomers of $Cu_2(OH)_3Cl$ undergo antiferromagnetic phase transition at different low temperatures, and possess apparent geometric frustration features,[1−4] our continued investigations have shown that almost all of the hydroxyl transition metal halides $M_2(OH)_3X$($M$ = Mn, Fe, Co, Ni, Cu; $X$ = Cl, Br, I) exhibit geometric frustration properties to some extent.[5] Several related new phenomena have been found, such as the coexistence of long-range order and spin fluctuation in γ-$Cu_2(OH)_3Cl$,[6] and the coexistence of ferromagnetic order and disorder in a uniform system of β-$Co_2(OH)_3Cl$;[7] the defect-induced short-range order from a spin-ice related state in deformed pyrochlore β-$Co_2(OH)_3Cl$,[8] and the drastic anion substitution effect in $Co_2(OH)_3Cl_{1-x}Br_x$.[9−11] Recent reports of nuclear magnetic resonance (NMR) studies on β-$Co_2(OH)_3Cl$ have demonstrated the difficulties in understanding the fundamental physics occurring at low temperatures in these geometrically frustrated materials, especially in β-$Co_2(OH)_3Cl$ and β-$Co_2(OH)_3Br$.[12−16]

To solve the basic magnetism problems, the exact crystal structure and its parameter changes at different temperatures have always needed to be made clear. Fortunately, because mid-infrared (IR) spectroscopy and Raman spectroscopy are sensitive to atomic vibration spectra, they can help to determine the constitution, crystal structure and the symmetry from the lattice vibration mode assignation.[17−20] We believe that studies on the temperature-dependent lattice vibration spectra (mid-IR and Raman) of magnetic materials will enable their magnetic properties to be demonstrated,[21−23] including the magnetic geometric frustration through the spin-lattice/phonon coupling effect,[24] especially at low temperatures when the geometric frustration property manifests itself.

*Project supported by the Grant-in-Aid for Scientific Research from the Japanese Society for the Promotion of Science (Grant No. Kiban-B 19340100) and the Grant-in-Aid for Scientific Research on Priority Areas from the Ministry of Education, Culture, Sports, Science and Technology, Japan (Grant No. Tokutei 22014008).

†Corresponding author. E-mail: zjcxdl@163.com

© 2011 Chinese Physical Society and IOP Publishing Ltd

Because the study of the preparations and magnetic measurements of β-$Co_2(OH)_3Cl$ and β-$Co_2(OH)_3Br$ became attractive only in recent years, until now (to the best of our knowledge) no Raman and IR spectra have been reported, even at room temperature (RT).

This article reports the Raman and mid-IR spectra of β-$Co_2(OH)_3Cl$ (Neel temperature $T_N$ = 10.5 K and the abbreviation L–Cl hereafter)and β-$Co_2(OH)_3Br$ (Néel temperature $T_{N1/2}$ = 6.2/4.8 K and the abbreviation L–Br hereafter) at RT, and assign the lattice vibration modes as precisely as possible in order to give the relationship between their spectral properties and microstructure, and provide useful information for further low-temperature magnetic-related spectral researches.

## 2. Materials and methods

### 2.1. Sample preparation

The polycrystalline β-$Co_2(OH)_3Cl$ and β-$Co_2(OH)_3Br$ (the abbreviation L–Cl/Br hereafter) samples were synthesised from solution reactions of appropriate quantities of $CoCl_2$/$CoBr_2$ and NaOH at around 200°C for several hours, respectively. The sediments were then washed thoroughly with purified $H_2O$ water to remove other solvable chemicals.[7] Deuterized samples $Co_2(OD)_3Cl$ and $Co_2(OD)_3Br$, which help to determine the O–H distances, were also prepared by the same hydrothermal method using the appropriate quantity of $CoCl_2$/$CoBr_2$, NaOD and $D_2O$ water.[7]

### 2.2. Crystal structure measurement

The crystal structures of M–Cl/Br were determined by powder synchrotron X-ray diffraction at beam line BL02B2, Spring-8 (Japan) and neutron powder scattering measurements were conducted at HERMES, JAERI (Japan) using the wavelength of 1.8143 Å.[7] Among these structural parameters, O–H distances are the O–D distances which can only be determined exactly by neutron powder scattering measurements using the deuterized samples β-$Co_2(OD)_3Cl$ and β-$Co_2(OD)_3Br$.

### 2.3. Mid-IR spectroscopy

Mid-IR (from 4000 to 400 $cm^{-1}$) absorption spectra were obtained using Bruker Vector 22 FTIR spectrometers with a resolution ratio of 2 $cm^{-1}$, and measurement using normal KBr disc technology at RT.

### 2.4. Micro-Raman spectroscopy

Raman spectra were obtained using HR800 HORIBA Jobin Yvon Laser micro-Raman microscopy equipped with 10×, 50× and 100× objectives. A small amount (about 1 mg) of powder samples were placed on the surface of a normal glass slide in air at RT, and their Raman spectra were excited by a Spectra-Physics model 127 $Ar^+$ laser (488.0 nm) with a resolution of 0.5 $cm^{-1}$ between 95 and 4000 $cm^{-1}$. Repeated acquisitions using the highest magnification were accumulated to improve the signal-to-noise ratio in the spectra. As the samples might be broken down to other chemicals at an intensive laser power density, 22 mW and 100× objective were used to obtain relatively strong Raman signals. Both Raman shift spectra were automatically baseline corrected, smoothed and normalized according to the largest counting peak value. As a conventional rule, only the integral parts of all the wavenumber data are used in the following.

## 3. Results and discussion

### 3.1. Crystal structural parameters

Figure 1 shows the crystal structure of L–Cl/Br, where the magnetic ions of $Co^{2+}$ form a three-dimensional network of linked tetrahedrons that can be viewed as alternating stacked layers of triangular lattice planes (T-planes) and kagome lattice planes (K+/K− planes) in the [001/00$\bar{1}$] directions.[7–9] The related structural parameters refined recently are collected in Table 1.[7–10]

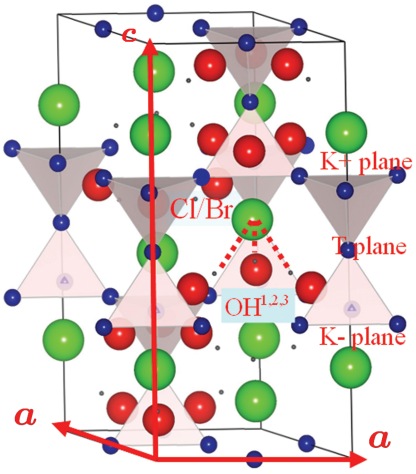



**Fig. 1.** (colour online) Crystal structure of β-$Co_2(OH)_3Cl$/Br.

**Table 1.** Relevant crystal structural parameters in units of Å of L–Cl and L–Br at RT.

| Parameter | L–Cl | L–Br |
|---|---|---|
| $a$ | 6.8370 | 6.9717 |
| $c$ | 14.4965 | 14.6635 |
| $d$(O–H) | 0.967(3) | 0.969(3) |
| $d$($Co^{K,K}$) | 3.4185 | 3.4858 |
| $d$($Co^{T,K}$) | 3.1198 | 3.1659 |
| $d$(Cl/Br–$Co^{K+}$) | 2.5986 | 2.6998 |
| $d$(Cl/Br–$Co^{T}$) | 4.0135 | 4.0763 |
| $d$(Cl/Br–H) | 2.312(3) | 2.341(3) |
| $d$(Cl/Br–O) | 3.1771 | 3.2273 |
| $d$(O–$Co^{K}$) | 2.0785 | 2.0840 |
| $d$(O–$Co^{T}$) | 2.1060 | 2.1366 |

From the obtained crystal structural parameters of L–Cl/Br, one can determine that their space group is rhombohedral $R\bar{3}m$ (No. 166), which has a very high symmetry relative to those of the three isomers of $Cu_2(OH)_3Cl$. In addition, the height of the tetrahedron along the $c$-axis is slightly smaller than that of the regular tetrahedron.

According to the common mean ion radius $R^0$ data,[25] $R^0(Co^{2+})$ = 0.74 Å, $R^0(O^{2-})$ = 1.40 Å, $R^0(Cl^-)$ = 1.81 Å, $R^0(Br^-)$ = 1.96 Å, one can give the following points about the relationship between the inter-atomic interaction and the inter-atomic distance necessary for spectral analysis.

1) The Co–O/Cl/Br interactions are relatively strong if the distance $d$($Co^{2+}$–$O^{2-}$) ≤ $d^0$($Co^{2+}$–$O^{2-}$) = 2.14 Å, $d$($Co^{2+}$–$Cl^-$) ≤ $d^0$($Co^{2+}$–$Cl^-$) = 2.55 Å, or $d$($Co^{2+}$–$Br^-$) ≤ $d^0$($Co^{2+}$–$Br^-$) = 2.70 Å.

2) A typical hydrogen bond (H-bond) may be formed if $d$($O^{2-}$–$Cl^-$) approaches $d^0$($O^{2-}$–$Cl^-$) = 3.21 Å or $d$($O^{2-}$–$Br^-$) approaches $d^0$($O^{2-}$–$Br^-$) = 3.36 Å when the angle $\theta$(O–H–Cl) or $\theta$ (O–H–Br) is larger than 120°.

One can conclude the following about their crystal structure features (CSF):

1) In a primitive cell of L–Cl, there is only one OH environment with $d$(O–H)= 0.967 Å and $d$(Cl–O) = 2.1771 Å, $\theta$(O–H–Cl) = 159.1(3)°. Therefore, a typical trimeric H-bond ($Co_3 \equiv OH)_3 \cdots Cl$ (or $(OH)_3 \cdots Cl$) may be formed, which has been recently demonstrated in β-$Co_2(OH/D)_3Cl$.[26–28]

2) In a primitive cell of L–Br, there is also only one OH environment with $d$(O–H)= 0.969(3) Å and $d$(Br–O)=3.2273 Å, $\theta$(O–H–Br) = 159.8(3)°. Therefore, the typical trimeric H-bond $(OH)_3 \cdots Br$ may be formed too.

3) For L–Cl/Br, every OH group bridges three Co ions, but has two kinds of Co–O distance: $d$($Co^{K-}$–O) = 2.078 Å and $d$($Co^{T}$–O) = 2.106 Å, which are all less than $d^0$(Co–O), and indicate that all O ions are strongly bonded to their nearest-neighbour Co ions.

4) Every Cl/Br ion, like the O ion, bridges three Co ions too, and all of the three $d$(Co–Cl/Br) are the same and less than $d^0$(Co–Cl/Br), so every Cl/Br is also strongly bonded to the Co ions.

5) There are two crystallographically independent Co ions that display characteristically distorted octahedral coordination geometry $Co^TO_4Cl_2/Br_2$ and $Co^KO_6$, i.e., $Co^T$ is bonded to four OH groups and two Cl/Br ions, and $Co^K$ to six OH groups without Cl/Br ion.

As to the difference between the CSFs of L–Cl and L–Br, one can conclude as follows:

6) Both distances between skeleton Co ions become larger for L–Br, but the change rates are within 2%.

7) The distances $d$($Co^K$–O) and $d$($Co^T$–O) in L–Br become slightly larger (0.3% and 1%) than those in L–Cl, respectively.

8) There is $d$($Co^{K+}$–$Br^-$) > $d$($Co^{K+}$–$Cl^-$), and the difference $d$($Co^{K+}$–$Br^-$)–$d$($Co^{K+}$–$Cl^-$) is less than $\Delta R^0$($Br^-$–$Cl^-$) = $R^0$($Br^-$) − $R^0$($Cl^-$) = 0.15 Å. This may imply the relatively strong Br–Co bond intensity (vibration force constant $k$).

## 3.2. Whole spectral profiles

Figures 2(a) and 2(b) show the normalized mid-IR transmittance spectra and the Raman shift spectra, respectively, in the whole 4000–0 $cm^{-1}$ region, although there are no data in the 400–0 $cm^{-1}$ region for the mid-IR spectra and 95–0 $cm^{-1}$ region for the Raman spectra.

According to the general spectral analysis method, the IR and Raman spectra are usually divided into two main ranges from higher to lower frequencies: functional group (FG) and finger-print (FP) regions, and the latter is more complicated and regarded to be difficult to analyse correctly.

According to the known information about L–Cl/Br, the following IR absorption bands and Raman shift peaks will appear: OH-related modes, Co–O related modes, Co–Cl related modes, lattice modes and sum/difference/overtones. Here, we can divide the spectra into three parts, as shown in the following corresponding sections. In order to perform the compar-

ative analysis and show intuitively the relationships between absorption and Raman spectra in the corresponding vibration regions, some parts will be amplified when needed.

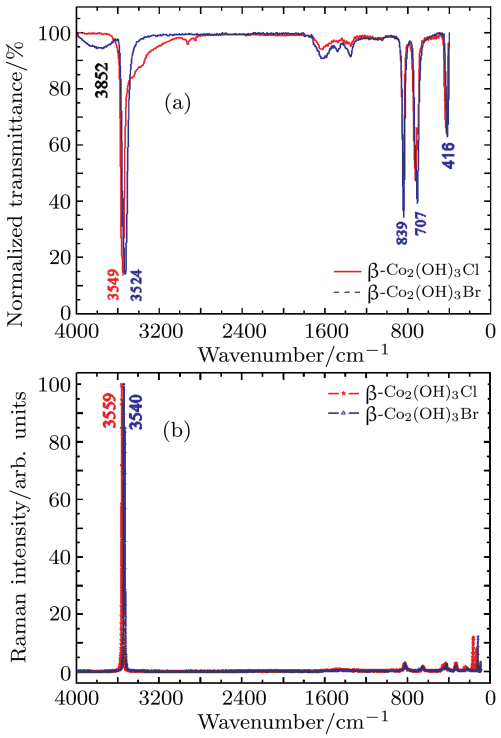



**Fig. 2.** (colour online) (a) Mid-IR absorption and (b) Raman spectra of β-$Co_2(OH)_3Cl/Br$.

## 3.3. Hydroxyl group (OH) vibrations

According to the above-mentioned crystal structure feature 1), one expects only one Raman peak and one IR absorption band in the same positions of the normal hydroxyl FP region because the single OH stretching vibration mode is always both IR active and Raman active, as shown in Fig. 2. However, after we amplify the 3650–3400 cm$^{-1}$ parts of Fig. 3, there are in fact two bands/peaks, although they are very near. According to Ergun *et al.*[29] Lagaron,[30] and Hase,[31] one can safely assign the L–Cl IR bands 3566/3549 cm$^{-1}$, L–Br IR bands 3548/3524 cm$^{-1}$, L–Cl Raman peaks 3559/3546 cm$^{-1}$, L–Br Raman peaks 3540/3528 cm$^{-1}$, as the Davydov splittings of the hydroxyl stretching vibration mode $\nu$(O–H), respectively.

Therefore, one can also simply consider their average values of IR bands 3558/3536 cm$^{-1}$, Raman peaks 3553/3534 cm$^{-1}$ as the single $\nu$(O–H) of L–Cl/Br, respectively. From Fig. 3, one can also see the following spectral properties.

(i) The band/peak difference of about 20 cm$^{-1}$ between their $\nu$(O–H) may imply that $d$(OH) of L–Br may be about 0.002 Å longer than that of L–Cl according to the famous relationship 5–12 cm$^{-1}$/0.001Å,[32] although the experimental data may not correctly reflect the difference because of the intrinsic experimental resolution power of 0.003 Å. Therefore, one can conclude that there is arelatively strong trimeric H-bond $(OH)_3\cdots Br$, while the larger $d$(Co–O) just shortens $d$(OH) in L–Br.

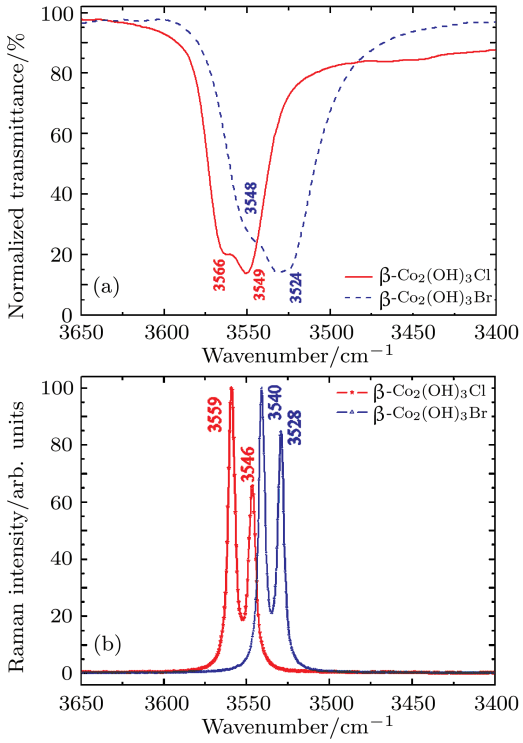



**Fig. 3.** (colour online) (a) IR absorption and (b) Raman spectra in the 3700–3100 cm$^{-1}$ range of $Co_2(OH)_3Cl/Br$.

(ii) According to the biatomic vibration frequency's formula $\nu = 1303(k/\mu)^{1/2}$ cm$^{-1}$, where $k$ is in units of mdyn/Å (1 mdyn/Å = 100 N/m) and $\mu$ is the reduced atomic weight with no dimension,[17] one can have $k$(OH) as strong as 7.0/6.9 mdyn/Å for L–Cl/Br.

As a useful spectral analysis method, the FP (OH in this paper) correlating peak (CP) assignment may now be done to obtain evidence or proof for the FP stretching modes. Because the Co–O and Co–Cl/Br related vibration modes are normally observed at wavenumbers less than 600 cm$^{-1}$ (the reason will be seen later), all the intrinsic L–Cl/Br IR bands and Raman peaks in the clear 1000–600 cm$^{-1}$ window can be assigned to the Co–O–H deformation modes $\delta$(Co–O–H). Therefore, we enlarge the remain-

ing 1000–50 $cm^{-1}$ part of all the spectra, as shown in Figs. 4(a) and 4(b). According to the fact that there are two kinds of Co–O–H with a relatively small H-bond H$\cdots$Cl/Br effect, one can assign the L–Cl IR bands 843/723 $cm^{-1}$, L–Br IR bands 839/707 $cm^{-1}$, and L–Cl Raman peaks 828/654 $cm^{-1}$, L–Br peaks 822/655 $cm^{-1}$ to hydroxyl deformation modes (both IR and Raman active) $\delta(Co^K–O–H)$ and $\delta(Co^T–O–H)$, respectively; and this CP assignment has been firmly supported by the recent comparative study on the vibration spectroscopy of $Co_2(OH)_3Cl$ and $Co_2(OD)_3Cl$.[27] Here, the L–Cl IR shoulder bands 738/702 $cm^{-1}$ and L–Br 729 $cm^{-1}$ may be caused by the difference-frequency, the sum-frequency or the overtone of some fundamental modes, and further investigation is needed to determine whether extra small L–Cl Raman peaks 691 $cm^{-1}$ and L–Br 689 $cm^{-1}$ are intrinsic in pure samples.

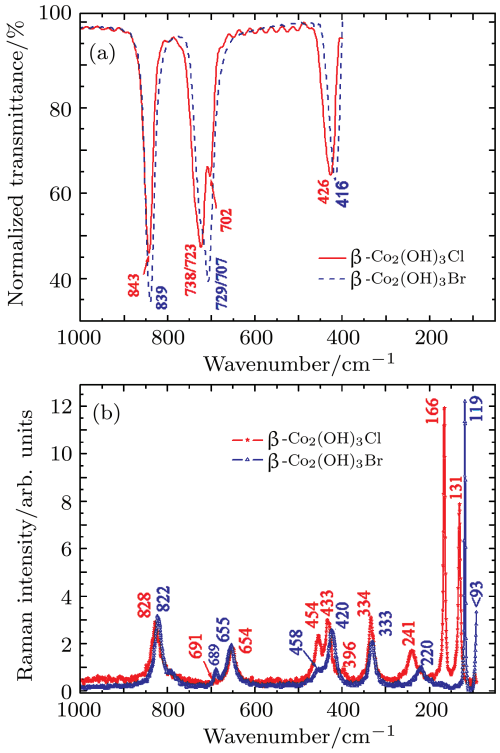



**Fig. 4.** (colour online) (a) IR absorption and (b) Raman spectra in the 1000–50 $cm^{-1}$ range of $Co_2(OH)_3Cl/Br$.

One can estimate the rate $\delta$(Co–O–H) and $\nu$(O–H) of L–Cl/Br to be about one-fifth to one-quarter.

From Fig. 2, one can see that except for the main IR bands of L–Cl/Br, the other bands larger than 1000 $cm^{-1}$, which vary with the experimental conditions, may be caused by the $CO_2$ and residual water in the KBr discs of FTIR disc technology, or, the sum-frequency, the difference-frequency and the overtones of some fundamental frequencies.

### 3.4. Co–O vibrations

From Fig. 4(b), one can observe that three Raman peaks in each spectrum are almost Cl/Br independent in the high wavenumber part of the general FP region (less than 600 $cm^{-1}$); therefore, most of them can be assigned to Co–O vibration modes. Although each spectral structure in this part seem to be very simple, it is still not easy to correspond these peaks to the precise vibration manners because of these periodical crystalline networks, unlike the isolated molecules in gas phase. Here, we adopt the simpler and more intuitive representation, which is the famous linear triatomic O–Co–O representation (we call it L-representation and do not use the viewpoint of $Co^KO_4Cl_2/Br_2$ and $Co^TO_6$ according to CSF5).[17]

In the L-representation for a symmetric linear triatomic unit $X$–$Y$–$X$, the wavenumber of the Raman active symmetric stretching mode can be given by

$$\nu_s(X-Y-X)=\frac{1}{2\pi c}\sqrt{\frac{k}{m_X}}, \tag{1}$$

where $c$ is the light speed in vacuum, $k$ is the force constant between the $XY$ ions and $m_X$ is the mass of the $X$ ion. If $k$ and $m_X$ are in units of mdyn/Å and the atomic quantity of $X$, respectively, Eq. (1) may be expressed as

$$\nu_s(X-Y-X)=1303\sqrt{\frac{k}{m_X}}(\mathrm{cm}^{-1}), \tag{2}$$

where $k$ varies with the distance $d_{XY}$, for example, $k\approx k_0(d_{XY}-d_0)^{-6}$ for most kinds of units bound weakly by van der Waals force.[32] For the IR active antisymmetric stretching mode, its wavenumber can be expressed as

$$\nu_{as}(X-Y-X)=1303\sqrt{\frac{k}{\mu}}(\mathrm{cm}^{-1}), \tag{3}$$

where $\mu=m_Xm_Y/(2m_X+m_Y)$ is the reduced mass. Therefore, one can see that an observable distance difference caused by the surrounding $X$ ions can lead to different Raman and IR bands.

If one uses the L-representation, L–Cl Raman peaks 454/433 $cm^{-1}$ are assigned to two kinds of O–Co–O symmetric stretching modes $\nu_s(O–Co^K–O)$ ($d$(O–$Co^K$) = 2.078 Å) and $\nu_s(O–Co^T–O)$ ($d$(O–$Co^T$) = 2.106 Å), respectively. This assignment is self-consistent with the relationships between wavenumber and distance, between wavenumber-separation and distance-difference, and between peak-intensity and

bond-number. Then Raman peaks 334/241 $cm^{-1}$ in L–Cl are regarded as the corresponding bending/deformation modes $\delta$(O–$Co^{K/T}$–O), and the IR band 426 $cm^{-1}$ in L–Cl is assigned to the O–Co–O asymmetric stretching modes $\nu_{as}$(O–$Co^{K}$–O), while $\nu_{as}$(O–$Co^{T}$–O) may be less than 400 $cm^{-1}$ and cannot be observed using the Bruker Vector 22. However, this representation can demonstrate self-consistently the small separation between $\nu_s$(O–$Co^{K}$–O) and $\nu_s$(O–$Co^{T}$–O), and the large difference between $\delta$(O–$Co^{K}$–O) and $\delta$(O–$Co^{T}$–O).

One can continue to use the formula $\nu$(O–$Co^{K/T}$–O) = $1303(k/m_O)^{1/2}$ $cm^{-1}$ in L-representation to estimate the force constants $k$($Co^{K/T}$–O) to be 1.98/1.74 mdyn/Å, which correspond reasonably to the $OH^-$ valence value of the hexa-coordinated $Co^{2+}$ figuration. In addition to this $k$($Co^{K/T}$–O) estimation, the fact that the bending mode $\delta$(O–$Co^{K/T}$–O) values are slightly larger than half of $\nu_s$(O–$Co^{K/T}$–O) agrees well with most examples in Ref. [17].

Similarly, one can assign Raman peaks 458/420 $cm^{-1}$ and 333/220 $cm^{-1}$ in L–Br to two kinds of $\nu_s$(O–$Co^{K/T}$–O) and $\delta$(O–$Co^{K/T}$–O) in the L-representation, respectively. In the meanwhile, the L–Br IR band 416 $cm^{-1}$ is assigned to $\nu_{as}$(O–$Co^{K}$–O) in the L-representation.

## 3.5. Co–Cl/Br vibrations

Following the above-mentioned assignment and using the L-representation only, one can assign the L–Cl Raman peak 166 $cm^{-1}$ and L–Br Raman peak 119 $cm^{-1}$ to the symmetric stretching modes $\nu_s$(Cl–$Co^{K}$–Cl) and $\nu_s$(Br–$Co^{K}$–Br), respectively. The reasonability of this assignment can be demonstrated by the reasonable $k$($Co^{K}$–Cl) = 0.58 mdyn/Å and $k$($Co^{K}$–Br) = 0.67 mdyn/Å for the $d$($Co^{K}$–Cl) = 2.5986 Å $\approx d^0(Co^{2+}–Cl^-)$ = 2.55 Å and $d$($Co^{K}$–Br) = 2.6998 Å $\approx d^0(Co^{2+}–Br^-)$ = 2.70 Å (see the relationship 1) with $m_{Cl}$ = 35.45 and $m_{Br}$ = 79.9. Then Raman peak 131 $cm^{-1}$ may be assigned to the bending mode $\delta$(Cl–$Co^{K}$–Cl), and the $\delta$(Br–$Co^{K}$–Br) value must be close but less than 95 $cm^{-1}$.

The following statement may be useful for the assignment of $\nu$(Cl–Co–Cl): if $d$(Co–Cl)≥2.55 Å in some material (high spin $Co^{2+}$), for the hexa-coordinated $Co^{2+}$, the bond valence is less than 0.33, especially in our case of trimeric H-bond $(OH)_3\cdots Cl$, the $k$(Co–Cl) is usually less than 1, and therefore $\nu_s$(Cl–Co–Cl)< $1303 \times m_{Cl}^{-1/2}$ = 218 $cm^{-1}$. Therefore, almost all the assignments of > 220 $cm^{-1}$ Raman shift mode $\nu_s$(Cl–Co–Cl) and the IR absorption band assignment of $\nu_{as}$(Cl–Cu–Cl) > 319 $cm^{-1}$ for $\nu_{as}$(Cl–Co–Cl) = $1303(k/m_\mu)^{1/2}$ $cm^{-1}$ (reduced mass $m_\mu$ = 63.5 × 35.5/(63.5 + 2×35.5) = 16.76) may be wrong. Similarly, if $d$(Co–Br)≥2.70 Å in some material (high spin $Co^{2+}$), for the hexa-coordinated $Co^{2+}$, Raman $\nu_s$(Br–Co–Br)< $1303\ m_{Br}^{-1/2}$ = 145 $cm^{-1}$ and IR $\nu_{as}$(Br–Co–Br)< 273 $cm^{-1}$.

In the medium wavenumber region, there may be weak sum-frequency, difference-frequency and overtone modes, which cannot be easily recognized.

Table 2 gives the collection of the above-mentioned spectral data and the corresponding suggested band/peak assignment, not including the unimportant shoulder bands/peaks, possible weak sum-frequency, difference-frequency and overtone modes, etc.

As Nakamoto pointed out,[17] vibrational spectra of crystals must be interpreted with caution, especially in the low-wavenumber region. Therefore, the above-mentioned assignment still needs further confirmation or even modification, especially in the

**Table 2.** Mid-IR data, Raman data and suggested modes of L–Cl/Br with the wavenumber in unit of $cm^{-1}$.

| | Mid-IR | | | Raman | | |
|---|---|---|---|---|---|---|
| | L–Cl | L–Br | Sugg. mode | L–Cl | L–Br | Sugg. mode |
| FG region | 3566 | 3548 | Davydov splitted $\nu$(O–H) | 3559 | 3540 | Davydov splitted $\nu$(O–H) |
| | 3549 | 3524 | | 3546 | 3528 | |
| CP region | 843 | 839 | $\delta$($Co^{K}$–O–H) | 828 | 822 | $\delta$($Co^{K}$–O–H) |
| | 723 | 707 | $\delta$($Co^{T}$–O–H) | 654 | 655 | $\delta$($Co^{T}$–O–H) |
| FP region | 426 | 416 | $\nu_{as}$(O–$Co^{K}$–O) | 454 | 458 | $\nu_s$(O–$Co^{K}$–O) |
| | | | | 433 | 420 | $\nu_s$(O–$Co^{T}$–O) |
| | | | | 334 | 333 | $\delta$(O–$Co^{K}$–O) |
| | | | $\nu_{as}$(O–$Co^{T}$–O) | 241 | 220 | $\delta$(O–$Co^{T}$–O) |
| | | | | 166 | | $\nu_s$(Cl–$Co^{K}$–Cl) |
| | | | | 131 | | $\delta$(Cl–$Co^{K}$–Cl) |
| | | | | | 119 | $\nu_s$(Br–$Co^{K}$–Br) |

low-wavenumber region, where various kinds of lattice modes may exist, although our comparative study between β-$Co_2(OH)_3Cl$ and β-$Co_2(OD)_3Cl$ has proved the correctness of $\delta$ (Co–O-H) modes (600–900 $cm^{-1}$), slightly H-dependent Co–O related modes (200–500 $cm^{-1}$), and H-independent low wavenumber region (< 200 $cm^{-1}$).[27]

Although the difference between Cl and Br atoms has caused apparent changes of the Co–Co and Co–O distances, the respective mode wavenumbers almost remain unchanged, possibly because of the equilibrium activity of different OH···Cl and OH···Br H-bonds, while almost the same amount of Co–O distance difference in a primitive cell has resulted in a shift of even several tens of $cm^{-1}$, possibly partly because of the different force constants under the same H-bond effect. Our further low-temperature Raman spectral experiments, aimed at investigating the spin-lattice coupling related to the geometrically frustrated magnetic transition phenomenon, possibly may give useful clues to some vibration mode assignments.

# 4. Conclusions

In conclusion, mid-IR absorption and Raman spectra of β-$Co_2(OH)_3Cl$ and β-$Co_2(OH)_3Br$ have been measured to study the corresponding correlation between their vibrational spectral properties and crystal microstructures. Through the comparative analysis of the four spectra we categorically assign or tentatively suggest the vibrational modes of OH group, O–Co–O, Co–O and Cl/Br–Co–Cl/Br units. These results, obtained at room temperature, are necessary for further investigations of spectral changes caused by the spin-lattice coupling effect at their low magnetic transition temperatures.

In this paper, we did not use the standard and complex factor group analysis method to perform the spectral assignment. Therefore, further theoretical and experimental investigations are required.

# References


[1] Zheng X G and Otabe E S 2004 *Solid State Commun.* **130** 107

[2] Zheng X G and Xu C N 2004 *Solid State Commun.* **131** 509

[3] Zheng X G, Kawae T, Kashitani Y, Li C S, Tateiwa N, Takeda K, Yamada H, Xu C N and Ren Y 2005 *Phys. Rev.* B **71** 052409

[4] Zheng X G, Mori T, Nishiyama K, Higemoto W, Yamada H, Nishikubo K and Xu C N 2005 *Phys. Rev.* B **71** 174404

[5] Zheng X G and Nishiyama K 2006 *Physica* B **374–375** 156

[6] Zheng X G, Kubozono H, Nishiyama K, Higemoto W, Kawae T, Koda A and Xu C N 2005 *Phys. Rev. Lett.* **95** 057201

[7] Zheng X G, Kawae T, Yamada H, Nishiyama K and Xu C N 2006 *Phys. Rev. Lett.* **97** 247204

[8] Zheng X G, Hagihala M, Kawae T and Xu C N 2008 *Phys. Rev.* B **77** 024418

[9] Hagihala M, Zheng X G and Kawae T 2009 *Physica* B **404** 671

[10] Fujihala M, Hagihala M, Zheng X G and Kawae T 2009 *Physica* B **404** 674

[11] Zheng X G, Hagihala M, Fujihala M and Kawae T 2009 *J Phys.*: *Conf. Ser.* **145** 012034

[12] Kubo H, Zenmyo K, Tokita M, Hamasaki T, Hagihala M and Zheng X G 2008 *J. Phys. Soc. Jpn.* **77** 013407

[13] Zenmyo K and Tokita M 2009 *J. Magn. Magn. Mater.* **321** 2192

[14] Maegawa S, Oyamada A, Sato S, Nishiyama M, Itou T and Zheng X G 2009 *J Phys.*: *Conf. Ser.* **145** 012018

[15] Tokita M and Zenmyo K 2009 *J. Phys.*: *Conf. Ser.* **150** 042208

[16] Maegawa S, Oyamada A and Sato S **2010** *J. Phys. Soc. Jpn* **79** 011002

[17] Nakamoto K *Infrared and Raman Spectra of Inorganic and Coordination Compounds, 2009 Part A: Theory and Applications in Inorganic Chemistry* 6th ed (New York: John Wiley & Sons)

[18] Martens W, Frost R L and Williams P A 2003 *N. Jb. Miner. Abh.* **178** 197

[19] Frost R L, Martens W, Kloprogge J T and Williams P A 2003 *J. Raman Spectrosc.* **33** 801

[20] Frost R L 2003 *Spectrochimica Acta Part* A **59** 1195

[21] Bi C Z, Ma J Y, Zhao B R, Tang Z, Yin D, Li C Z, Yao D Z, Shi J and Qiu X G 2005 *J. Phys.*: *Condens. Matter* **17** 5225

[22] Macalik L, Maczka M, Solarz P, Fuentes A F, Matsuhira K and Hiroi Z 2009 *Opt. Mater.* **31** 790

[23] Maczka M, Sanjuan M L, Fuentes A F, Macalik L, Hanuza J, Matsuhira K and Hiroi Z 2009 *Phys. Rev.* B **79** 214437

[24] Fabreges X, Petit S, Mirebeau I, Pailhes S, Pinsard L, Forget A, Fernandez-Diaz M T and Porcher F 2009 *Phys. Rev. Lett.* **103** 067204

[25] Ionic Radius *Wikipedia, the free encyclopedia* http://en.wikipedia.org/wiki/Ionic_radius [2010-11-20]

[26] Liu X D, Hagihala M, Zheng X G, Tao W J, Meng D D, Zhang S L and Guo Q X *Chin. Phys. Lett.* **28** 017803

[27] Liu X D, Meng D D, Zheng X G, Hagihala M and Guo Q X 2011 *Adv. Mater. Research* **146–147** 1194

[28] Liu X D, Tao W J, Zheng X G, Hagihala M, Meng D D, Zhang S L, Guo Q X 2011 *Acta Phys. Sin.* **60** 037803 (in Chinese)

[29] Ergun H B, Gehring K A and Gehring G A 1976 *J. Phys.* C: *Solid State Phys.* **9** 1101

[30] Lagaron J M 2002 *Macromol. Symp.* **184** 19

[31] Hase Y 2006 *J. Braz. Chem. Soc.* **17** 741

[32] Novak A 1974 *Struct. Bonding* **18** 177